PERGAMON

International Journal of Multiphase Flow 28 (2002) 1853–1869

International Journal of Multiphase Flow

www.elsevier.com/locate/ijmulflow

Pinch-off modes and satellite formation in liquid/liquid jet systems

I.N. Milosevic *, E.K. Longmire

Department of Aerospace Engineering and Mechanics, University of Minnesota, 107 Akerman Hall, 110 Union St. SE., Minneapolis, MN 55455, USA

Received 4 April 2002; received in revised form 3 June 2002

Abstract

Forced jets of glycerin/water solution flowing into silicone oil were investigated. Forcing amplitudes were sufficient to induce stable or semi-stable pinch-off modes in the jet. The indices of refraction in the two liquids were matched, and planar slices of flow were visualized using laser induced fluorescence. Two-dimensional velocity fields were obtained by particle image velocimetry (PIV). For a viscosity ratio, $\eta_i/\eta_o = 1.6$, satellites form at lower Reynolds numbers as well as lower Strouhal numbers. Satellite occurrence depends on the interface shape approaching pinch-off as well as the detailed velocity gradients surrounding the pinch-off region. Satellite formation required a zone of concave curvature downstream of but close to the jet neck as pinch-off approached. This zone was associated with intense vorticity that first deformed the interface into an upstream-facing cone attached to the main drop and then deformed the cone into a satellite shape. Increasing the ambient viscosity suppressed satellite formation for the Reynolds and Strouhal numbers examined.

Keywords: Jet; Pinch-off; Satellites; PIV; LIF

1. Introduction

Injection of one fluid into another has been of great interest for many years. Liquid–gas and liquid–liquid jets can be found in many industrial applications including ink-jet printers, internal combustion engines, chemical reactors, oil–water separators and fuel atomizers. In liquid–liquid extractors used in chemical processing, emulsions of small droplets are generated in order to increase interfacial area and hence mass transfer. The size distribution of the droplets thus has a

* Corresponding author.

0301-9322/02/$ - see front matter
PII: S0301-9322(02)00046-0

direct effect on mass transfer rates. In ink-jet printers, droplets of uniform size are desired. A problem arises when small satellite drops form between the larger primary droplets during the pinch-off process. In both of these examples, it can be seen that the dynamics of pinch-off, including whether or not satellites form, directly affects system performance. In order to optimize and control performance, then, it is necessary to understand the mechanisms governing pinch-off.

Beginning with Lord Rayleigh, a number of researchers attempted to describe injection of liquid jets into air or another liquid using linear theory. Although a linear inviscid approximation works well in a number of cases (see the review by Meister and Scheele, 1967), it fails to predict satellite formation. Linear theory predicts drop formation corresponding with a dominant perturbation wavelength, and therefore only primary drops are allowed. Satellite drop formation results, however, from nonlinear behavior.

A number of studies have examined liquid satellites forming in air. Rutland and Jameson (1970) compared theoretical predictions and experimental results of primary and satellite drop size resulting from the breakup of capillary jets. They applied Yuen's (1968) nonlinear inviscid theory to third order to predict the volume of primary and satellite drops for wave numbers <0.7. For wave numbers >0.7, satellites appeared in the experiments, but the theory did not predict them. Subsequent perturbation analyses, always taken to second or third order, (see e.g. Nayfeh, 1970; Lafrance, 1975; Taub, 1976; Chaudhary, 1977; Pimbley and Lee, 1977; Scarlett and Parkin, 1977) did reasonably well at predicting experimental behavior. The review by Bogy (1979) provides a detailed comparison of the various analytical techniques and studies.

Pimbley and Lee (1977) examined the effect of sinusoidal velocity perturbations on satellite formation. The amplitude of the perturbation was proportional to an excitation current applied to a magnetostrictive actuator. Within the range of wavelengths studied, increasing the amplitude of the perturbation velocity suppressed satellite formation. Satellites were completely suppressed for $3 < \lambda/d < 8$. The wavelength that appeared to require the smallest perturbation amplitude was $\lambda/d \cong 6$. Chaudhary and Maxworthy (1980) used a piezoelectric actuator to perturb liquid jets in order to control satellite formation and merging. They used flow visualization to demonstrate two types of formation. In one, primary and satellite drops broke off alternately from the jet. In the other, a full 'wavelength' broke off from the jet and later split into larger and smaller drops. A combination of a fundamental frequency and the third harmonic were applied to control the direction of satellite merging. Also, they showed that by setting the third harmonic in phase with the fundamental, satellites could be eliminated.

Zhang and Basaran (1995) studied the influence of fluid properties on satellite formation in a dripping flow. In their flow, a thread formed between an evolving drop and a conical section upstream. The thread always broke first at the drop end, then (sometimes) at the cone end, to form a satellite. The length of the thread increased as liquid viscosity and flow rate increased. Kowalewski (1996) observed a similar trend for thread length in jets. 'Micro threads' upstream of droplets, which were observed down to a scale of 1 μm, broke long before molecular scales were reached. Micron-scale satellites were observed to form from these threads.

Many researchers, including Meister and Scheele (1969), Skelland and Walker (1989), Kitamura et al. (1982), Richards et al. (1993), and Webster and Longmire (2001) have investigated liquid–liquid jet systems, but in general, satellite formation was not examined in detail. Tjahjadi et al. (1992) performed experiments on the distribution of subsatellite and satellite drops generated from highly strained filaments in liquid/liquid systems. Lower viscosity ratios of inner to

outer fluid (e.g. 0.01) resulted in larger numbers of satellites formed compared with higher viscosity ratios. Boundary-integral calculations agreed very well with the experiments. Cohen et al. (1999) examined interface angles near pinch-off for liquids dripping into liquids over a range of viscosity ratios. Their results agreed very well with boundary integral calculations by Zhang and Lister (1999) and angles measured near primary drop pinch-off in jets by Longmire et al. (2001). Satellites were not examined in these experiments.

In this paper, we attempt to examine satellite drop formation and the accompanying dynamics as a function of several input parameters in a liquid/liquid jet system subject to periodic forcing. The jet Strouhal and Reynolds numbers were varied while the fluid properties were held constant. Evolving interface angles and topologies were examined by flow visualization, and velocity and vorticity fields were measured by particle image velocimetry (PIV). An index-matching technique (see Longmire et al., 1999) was applied to avoid optical distortion in the images and to allow for simultaneous velocity measurements in both liquids.

2. Experimental description

The experiments were performed in a closed-loop facility that consists of a tank, a pump, a control valve, a rotameter, and a forcing apparatus. A sketch of the facility is given in Fig. 1. The tank is 56 cm in height and 20.3 cm in cross-section. A magnetic-drive pump generates a steady flow that is controlled by a needle valve. The flow (a water/glycerin mixture) passes through a honeycomb straightener before exiting a nozzle into an ambient layer of Dow Corning fluid. The nozzle has exit diameter of 1 cm and a contraction ratio of 16.4:1. The contraction profile was generated from a third-order polynomial with zero slope and curvature at the inlet and outlet.

An audio speaker drives a piston attached to the flow loop that imposes sinusoidal perturbations on the mean velocity. The perturbations are controlled to generate repeatable pinch-off conditions.

At the top of the tank, was a layer of Dow Corning fluid 33 cm in height. The remainder of the tank was filled with the water/glycerin mixture (48% glycerin by volume). The glycerin fraction was chosen so that the indices of refraction of the mixture and Dow Corning fluid were matched. The fluid properties are given in Table 1. In all experiments, a small amount of Rhodamine 6G, which fluoresces under laser illumination, was added to the jet fluid, in order to distinguish it from the ambient. In PIV experiments, both fluids were seeded with titanium dioxide particles (1–3 μm in diameter) that acted as tracers. The interfacial tension between the fluids was measured as 29 mN/m.

Two single-pulsed Nd:YAG lasers and a continuous Argon ion laser were employed for illumination. The beams were directed through spherical and cylindrical lenses to generate vertical light sheets of 1 mm thickness at the test section. The pulse energy of each beam was 32 mJ for the Nd:YAG lasers. The Argon laser power was 0.55 W. Images for PIV were acquired by a Kodak Megaplus dual-frame camera with array size of 1008×1018 pixels and pixel depth of 8 bits. Instantaneous images of phase-locked flow were acquired with a Kodak DCS 420 M camera (1012×1524 pixels), and real-time image sequences were acquired with a NAC Memrecamci system (572×432 pixels) at 500 frames/s. Timing control signals were generated with a Macintosh

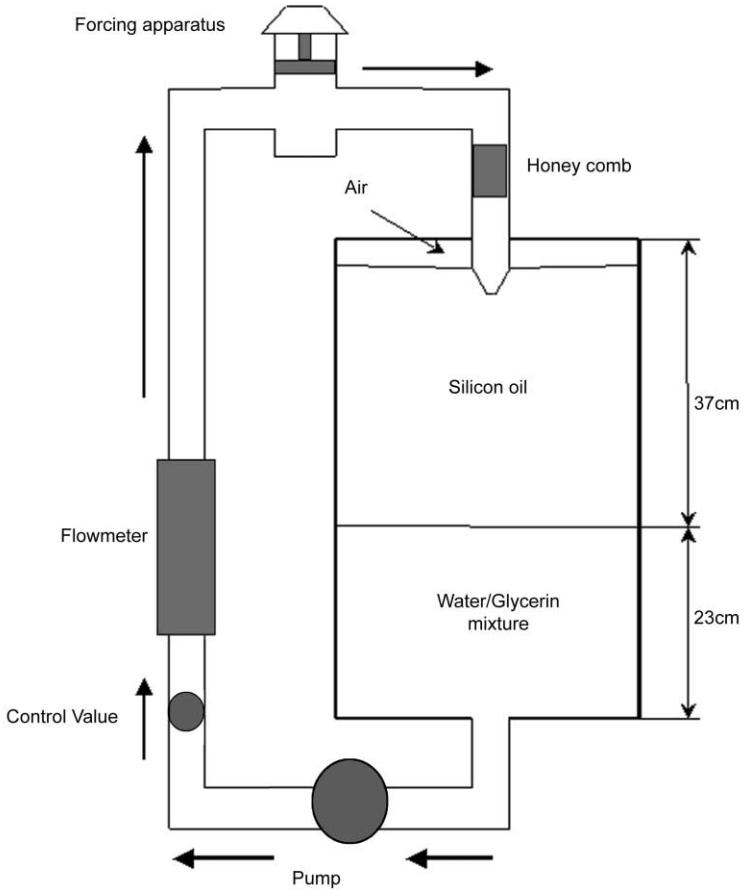

Fig. 1. Jet flow facility.

Table 1
Fluid properties

Fluid property	Density ρ (kg/m^3)	Dyn. viscosity η (kg/m s)
Ambient fluid (o) Dow Corning 200 fluid	920	4.6×10^{-3}
Jet fluid (i) water/glycerin (52/48% by volume)	1136.4	7.37×10^{-3}

computer and National Instruments NB-MIO-16X board. The signals were employed to drive the piston forcer, the camera, and the pulsed lasers.

Prior to PIV analysis, the images were preprocessed with custom software to remove the 'dyed' background as well as any coagulated particles. The PIV analysis was performed using a cross-correlation method within TSI Insight software. Interrogation areas were 64 by 64 pixels (equivalent to 0.73 mm $\times$ 0.73 mm in real space), and the areas were overlapped by 50%. The percentage of valid vectors in each image ranged from 98% to 100%. In the plots shown in Section 3, all velocity values are normalized by the nozzle exit velocity, and vorticity values are normalized by the ratio of nozzle exit velocity to exit diameter.

3. Results

The parameters chosen to describe the flow were the density ratio, the viscosity ratio, a Reynolds number based on the jet fluid and nozzle exit properties, a Strouhal number, a Bond number, and an Ohnesorge number:

$$\frac{\rho_i}{\rho_o}, \quad \frac{\eta_i}{\eta_o}, \quad Re = \frac{\rho_i U_e D_e}{\eta_i}, \quad St = \frac{fD_e}{U_e}, \quad Bo = \frac{\Delta\rho g D_e^2}{\sigma}, \quad Oh = \frac{\eta_i}{\sqrt{\rho_i D_e \sigma}},$$

where ρ is density, η is viscosity, subscripts i and o denote inner or jet fluid and outer or ambient fluid respectively. Subscript e denotes the condition at the nozzle exit. The forcing frequency, gravitational constant, interfacial tension and density difference between fluids are given by f, g, σ and $\Delta\rho$ respectively. In the experiments, the Strouhal number was varied between 1.43 and 5.53, and the Reynolds number was varied from 39 to 76 while the other quantities were held fixed ($Bo = 7.3$, $Oh = 0.013$). The forcing amplitude was also varied over a wide range to examine its effects on jet behavior. In general, the range of amplitudes that yielded an axisymmetric jet increased with increasing Reynolds number and Strouhal number. For the results shown, the amplitude was chosen just high enough to yield a stable repeatable pinch-off condition.

3.1. Characteristics of satellite formation

3.1.1. Flow visualization

After the jet exits the nozzle, it accelerates due to gravity and decreases in cross-section before it eventually pinches off. Increasing the forcing amplitude moves the pinch-off location upstream until at high enough amplitudes, a dripping mode results. Initially, we discuss two of the simplest cases observed over the range of parameters studied: $Re = 58$, $St = 3.5$ and $Re = 39$, $St = 3.5$. Forcing amplitudes, measured as the peak-to-peak voltage input to the speaker, were 2.4 and 2.6 V respectively. These amplitudes correspond to oscillation amplitudes of 8.6% for $Re = 58$ and 15.6% for $Re = 39$, in the volumetric flow rate at the nozzle exit. Amplitude in flow rate is defined as one half of the peak-to-peak variation. Pinch-off occurred at y/D of about 4.6 and 4 for $Re = 58$ and $Re = 39$ respectively. Sequences of phase-locked images for both cases are shown in Figs. 2 and 3. The phase shortly before pinch-off is set at $\Phi = 0°$.

For the case of $Re = 58$, $St = 3.5$ (see Fig. 2), satellites occur very rarely. In one experiment, they were observed once every 20 s on average. The forcing frequency, which equaled the pinch-off frequency, was 13 Hz. The very sharp jet tip and nearly flat upstream end of the drop characterize the interface shape just before pinch-off. The angle between the tip interface and horizontal plane (hereafter called the 'jet pinch-off angle') lies in the range 78–83°. The angle between the drop interface and the horizontal (hereafter called the 'drop pinch-off angle') was measured as 4–7°. At $\Phi = 20°$, the drop is fairly round, but in subsequent phases, the shape oscillates strongly. The drop first inverts very strongly on the upstream side (see $\Phi = 100°$) and later forms a distinct cusp (see $\Phi = 220°$) as the upstream interface rebounds. Additional visualization reveals that drop oscillations continue over a significant distance downstream. The relatively low ambient viscosity, thus, results in a slow damping of the oscillations.

After pinch-off, the jet tip stagnates until $\Phi = 220°$. During this period, fluid from above fills the tip such that a spherical shape develops ($\Phi = 80°$) and grows. The thick part of a wave

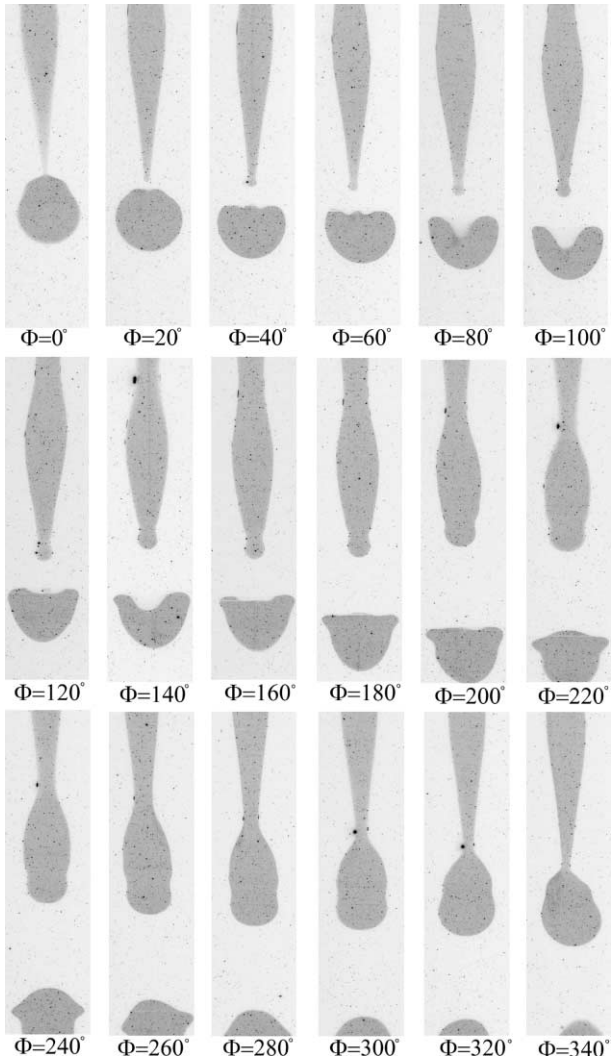

Fig. 2. Phase-locked sequence of jet pinch-off at $Re = 58$ and $St = 3.5$. Top edge of each image is $1.6D$ from the nozzle. Length of each image is $4.7D$.

upstream of the spheroid travels downstream while gradually transferring fluid to the jet tip. The thin part of the wave evolves into a neck, and the drop developing downstream maintains a region of inverted curvature up to the pinch-off phase. A significant fraction of the total volume (about 1/3 at $\Phi = 340°$) is contained in the upstream portion of the developing drop.

For the case of $Re = 39$, $St = 3.5$ (see Fig. 3), satellites always occurred, although their size varied over a period of about 1 s. The size and shape of the main drop varied correspondingly over the same period. The sequence in Fig. 3 represents an intermediate satellite size. At $\Phi = 0°$, the jet tip is blunter than in the previous case with the interface angled 65° above horizontal. The upstream end of the drop is relatively flat and nearly horizontal except for a cone-shaped structure

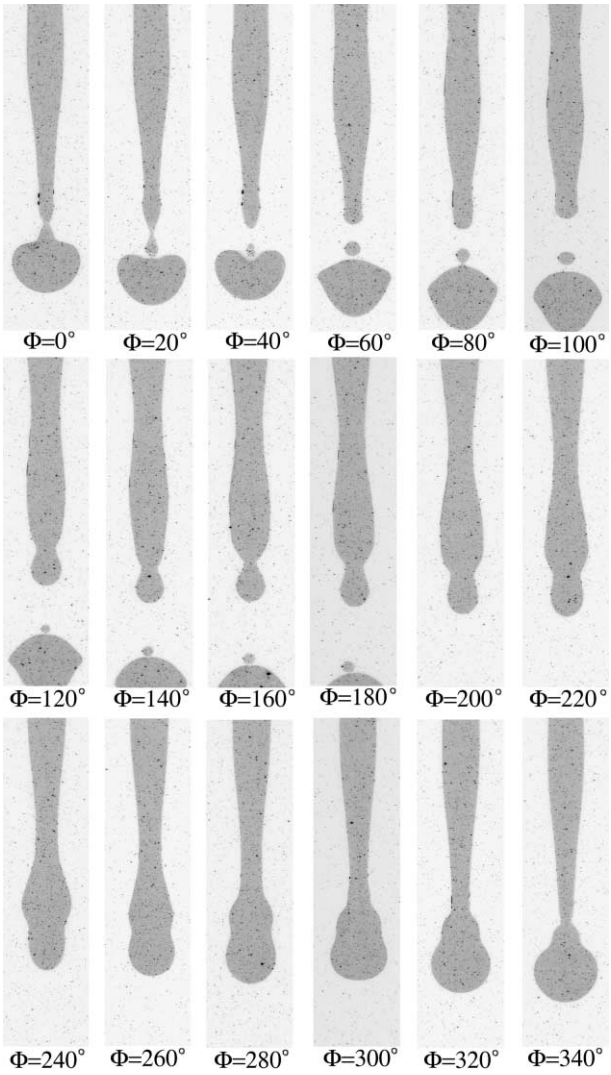

Fig. 3. Phase-locked sequence of jet pinch-off at $Re = 39$ and $St = 3.5$. Top edge of each image is $0.6D$ from the nozzle. Length of each image is $4.7D$.

centered on the axis. A sudden change in interface slope and curvature is visible where the cone intersects the drop. The angle between the cone interface near pinch-off and the horizontal is also about 65°.

In fact, the jet does not pinch-off above the cone (see the high-frame-rate sequence in Fig. 4). Instead, the cone evolves into a (satellite) drop shape as the interface of the primary drop downstream begins to invert. At this time, the interfaces upstream and downstream of the eventual break point appear to be rotating in opposite directions. The satellite then breaks off of the primary drop (see also Fig. 3, $\Phi = 20°$). Finally, a relatively long, thin thread develops

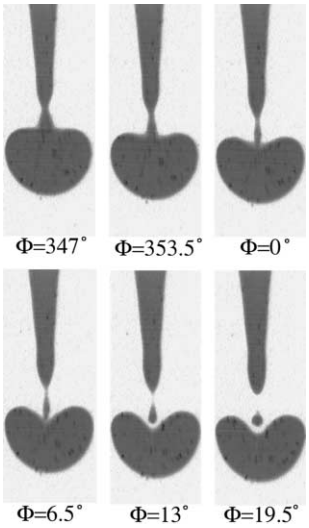

Fig. 4. High-frame-rate sequence of jet pinch-off at $Re = 39$, $St = 3.5$. Top edge of each image is $2.75D$ from the nozzle. Length of each image is $2.12D$.

between the satellite and jet tip before the satellite pinches off. Similar threads have been observed by other researchers examining liquid pinch-off in air (Zhang and Basaran, 1995; Kowalewski, 1996). A second possible behavior (which is much less frequent and therefore not shown) occurs when the cone detaches first from the jet and then from the main drop to form a satellite. For this mode, the final detachment from the main drop and the associated pinch-off angles have been difficult to observe thus far.

At $\Phi = 20°$ (Fig. 3), the upstream end of the primary drop is clearly inverted in contrast to the same phase for $Re = 58$. Note also that the jet interface contains two axisymmetric waves of differing wavelength. At $\Phi = 40°$, the satellite has detached completely, and the inversion of the upstream end of the main drop has increased. This indicates that the fluid in the upstream part of the drop is moving faster than the fluid downstream, resulting in axial compression. The maximum inversion of the drop is weaker than for $Re = 58$, and the drop oscillates back to a convex shape at an earlier phase.

In this case, the tip of the jet recoils immediately after satellite pinch-off in order to decrease the local curvature. Similar to $Re = 58$, the tip does not advance downstream over several of the phases shown. However, the jet tip in this case remains blunter than for $Re = 58$. Again, fluid flowing from above increases the local radius and volume near the tip. Also, the thick part of the upstream wave advances toward the tip, but stops short as a spherical end grows. At $\Phi = 160°$, it appears that the spherical section will pinch-off from the main column, but it does not. Instead, the spherical end proceeds to increase its volume considerably while the maximum jet diameter remains fixed through $\Phi = 280°$. Then, the neck between the jet column and the forming drop narrows so that less liquid flows into the drop. The drop shape continues to evolve so that the downstream part dominates the total volume (about 96% of the total volume at $\Phi = 340°$). The upstream part decreases in volume, eventually forming the small cone described above.

3.1.2. PIV results

The behavior discussed above was investigated separately by examining velocity characteristics from PIV measurements. Fig. 5 shows two samples of PIV images where both liquids are seeded with titanium dioxide particles. The vector fields resulting from PIV image pairs were interpolated to determine contour plots of axial velocity and vorticity for the two cases described above. In Figs. 6 and 7, positive axial velocity points downward. Note that, as in Figs. 2 and 3, the results presented are derived from phase-locked as opposed to real-time sequences.

In Fig. 6, we can see that, before pinch-off ($\Phi = 320°$), the maximum axial velocity is located approximately at the jet neck. The fluid is thus accelerating into the neck and acting to increase the volume of the drop. As pinch-off is approached, the maximum moves downstream into the drop (see $\Phi = 350.6°$ and 0°). At the neck, the axial velocity is increasing ($\partial u/\partial y > 0$) so that the radial velocity must be inward. The velocity pattern thus encourages the neck to pinch-off. After pinch-off, the axial velocity maximum near the upstream end of the drop is consistent with the axial compression and inward rotation of the upstream drop surface observed in Fig. 2.

The velocity plots for $Re = 39$, shown in Fig. 7, are more complex. Before pinch-off ($\Phi = 327.5°$), a velocity maximum also occurs at the jet neck. As the cone develops on the upstream end of the drop, however, the maximum moves into the cone (see $\Phi = 340.5°$) and strengthens so that the highest contour level plotted corresponds with $19U_e$. (The maximum level found in any of the $Re = 58$ plots is $17U_e$.) The axial acceleration inside of the cone must coincide with radial inflow, and the inflow causes the cone to shrink in size (see $\Phi = 347°$). Note also at this phase that the contours inside the cone become very closely spaced. The strong local velocity maximum next moves into the upstream end of the main drop. Here, the maximum contour level reaches $23U_e$. The axial acceleration immediately upstream of this location is very strong, and it distorts the interface inward, eventually causing the main drop to pinch-off.

After the pinch-off, the velocity maximum, which resides inside of the main drop, is diminished. The location of the maximum close to the drop center (in the axial direction) suggests that the upstream interface will not deform or invert much more than it has already. A local minimum in velocity occurs first near the satellite pinch-off point at $y/D = 4.05$ ($\Phi = 8°$). The local acceleration downstream of this point must act to break off the satellite. After this break, the jet tip velocity decreases significantly to $\sim U_e$ while the satellite drop velocity decreases to $\sim 5U_e$ compared with its velocity before breaking of $9U_e$.

Vorticity plots for the two flow cases are shown in Figs. 8 and 9. In Fig. 8 ($\Phi = 313°$), three centers of vorticity are present: one at the jet neck and two along the drop interface. The center

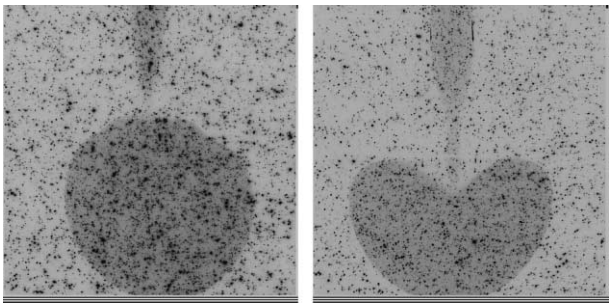

Fig. 5. PIV images of phase 0° at $St = 3.5$ and $Re = 58$ (left) and $Re = 39$ (right). Length of each image is $1.1D$.

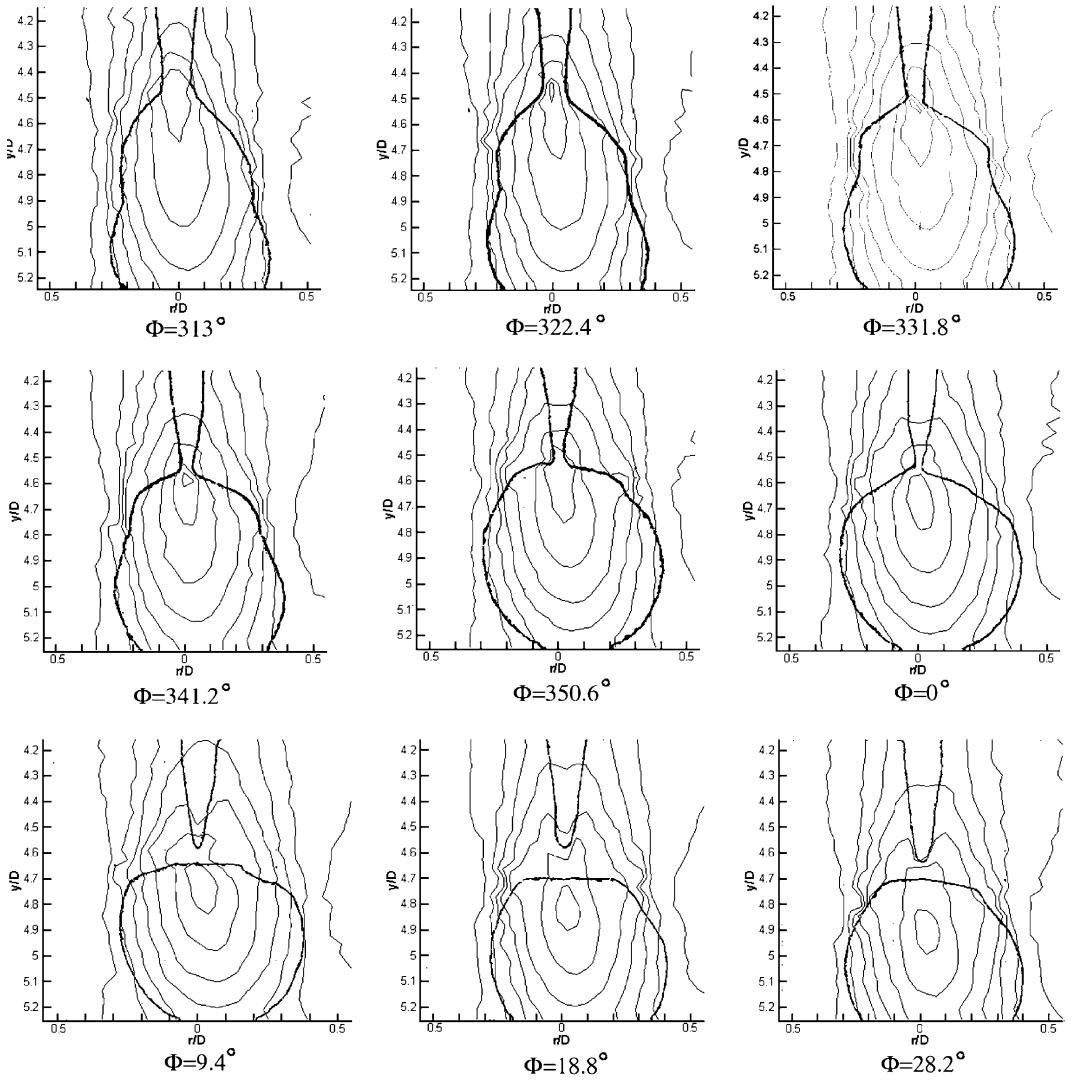

Fig. 6. Normalized axial velocity contours of forced flow at $St = 3.5$ and $Re = 58$. Lowest contour level is 1, and succeeding levels are incremented by 2.

near the upstream end of the drop and its concentration of vorticity act to rotate and flatten the interface and hence to encourage pinch-off. As the flow progresses to $\Phi = 350.6°$, the circulation at the jet neck weakens, and the two centers along the drop move closer together. The largest vorticity values are found outside of the drop interface at the location of the inverted curvature. This area of circulation persists through the pinch-off and remains attached to the drop that forms. After the drop pinches off, a small ring of inverted vorticity develops at the jet tip due to the recoiling interface there.

The $Re = 39$ case (Fig. 9) initially contains three vorticity maxima also, but they are spaced much more closely than in the $Re = 58$ case (see $\Phi = 327.5°$). The differences at this phase are

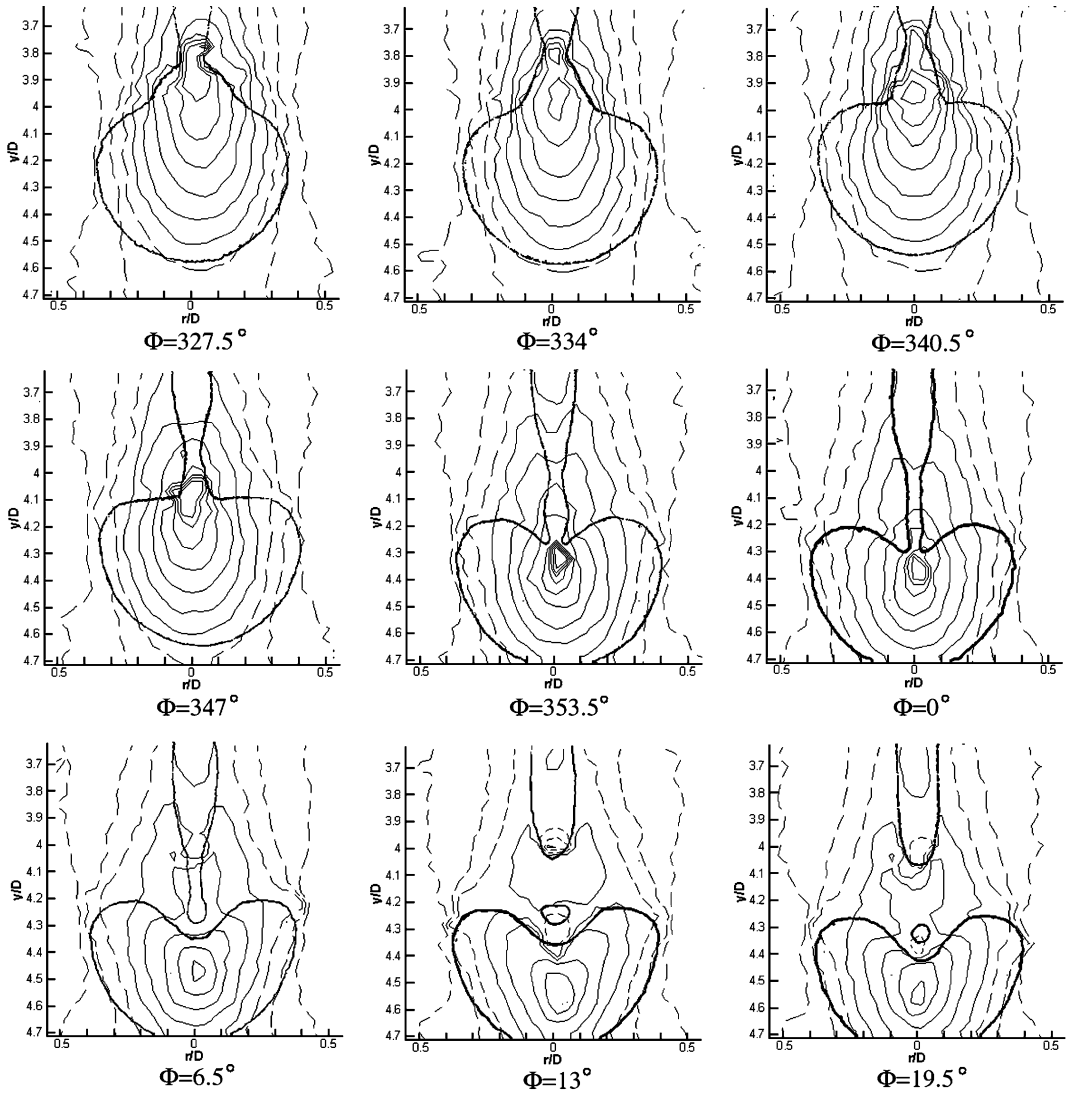

Fig. 7. Normalized axial velocity contours of forced flow at $St = 3.5$ and $Re = 39$. Lowest contour level is 1, and succeeding levels are incremented by 2.

important to notice, because ultimately they determine the interface shape evolution through pinch-off and whether or not a cone, and subsequently a satellite, will form. The maximum at the jet neck is very strong, and quickly dominates the center maximum which disappears upon formation of the cone shape ($\Phi = 334°$). The third maximum is focused at the junction of the cone and drop. Note that this vortex core is much closer to the jet axis and neck than when $Re = 58$. This core and the core at the jet neck also have larger maximum values and larger circulation than their counterparts when $Re = 58$. While the center at the neck of the cone dissipates, the center at the cone/drop interface intensifies ($\Phi = 340.5°$ and 347°). The strong rotation helps to drive fluid downward out of the cone, decreasing its volume (see $\Phi = 347°$). As the vortex core radius

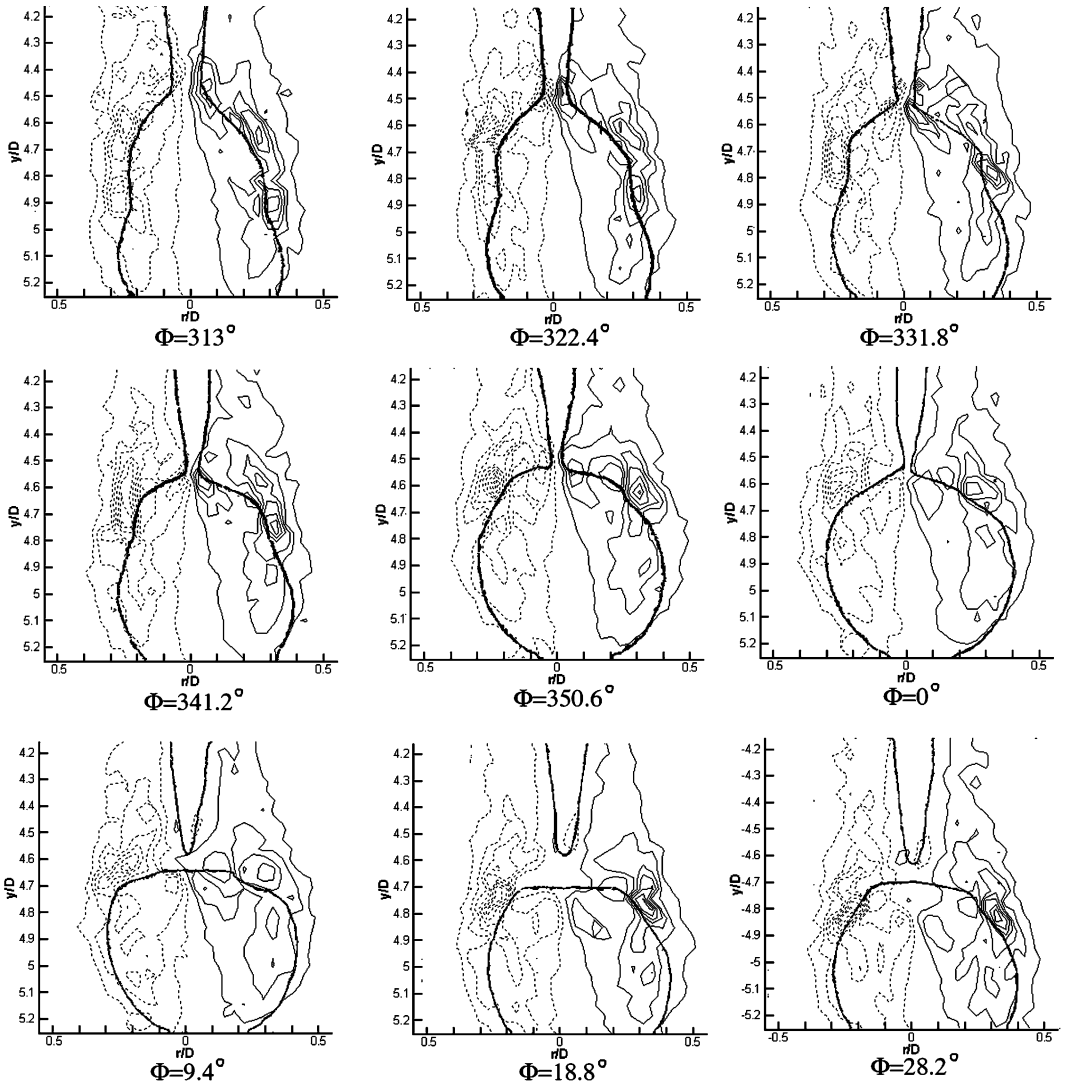

Fig. 8. Normalized vorticity fields of forced flow at $St = 3.5$, and $Re = 58$. Lowest contour level is 4, and succeeding levels are incremented by 4.

decreases, it propagates faster (and forward relative to the drop interface so that the center of vorticity moves inside of the developing drop ($\Phi = 353.5°$). The core acts to stretch and drag the drop interface downward, encouraging the eventual pinch-off.

After the drop pinch-off, two zones of reversed vorticity develop: one along the inverted drop interface, and one near the jet/satellite separation location. The first zone suggests that the drop has reached its maximum inversion and is starting to oscillate back toward a convex shape. The second zone is associated with the satellite pinch-off. After the pinch-off, the reverse vorticity at the jet tip intensifies as the tip recoils, causing the local curvature to decrease.

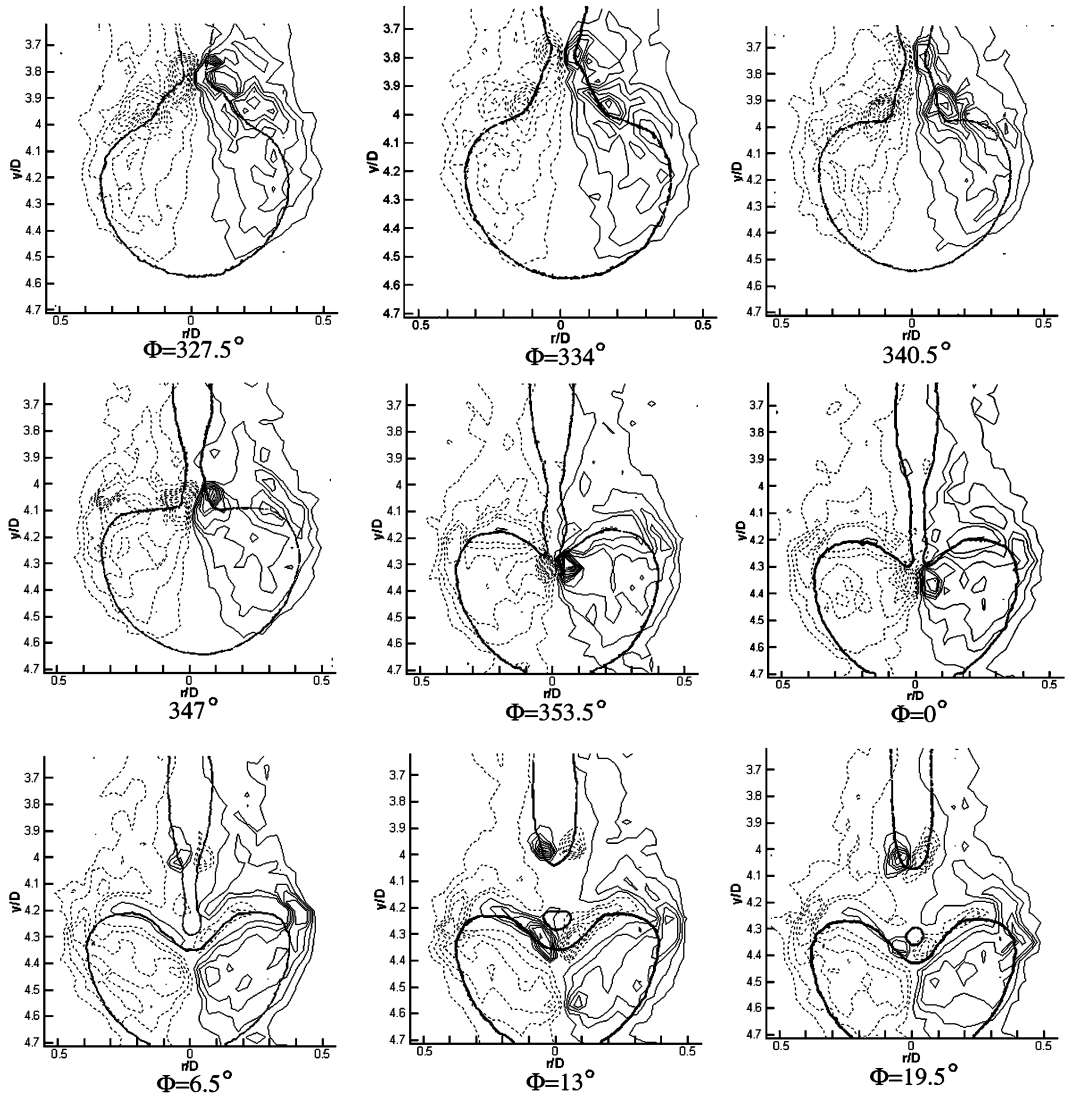

Fig. 9. Normalized vorticity fields of forced flow at $St = 3.5$, and $Re = 39$. Lowest contour level is 4, and succeeding levels are incremented by 4.

3.2. Effects of parameter variation

Many Reynolds/Strouhal combinations were observed in order to determine conditions under which satellites occurred. The results of these tests are plotted in Fig. 10. Several points are included from earlier tests using an outer fluid with significantly higher viscosity (48×10^{-3} kg/m s). Visualizations under these conditions can be found in Webster and Longmire (2001). The plot shows that lower Reynolds numbers encouraged satellite formation. Also, Strouhal numbers that were sufficiently low allowed the formation of satellites or drop pairs at higher Reynolds numbers.

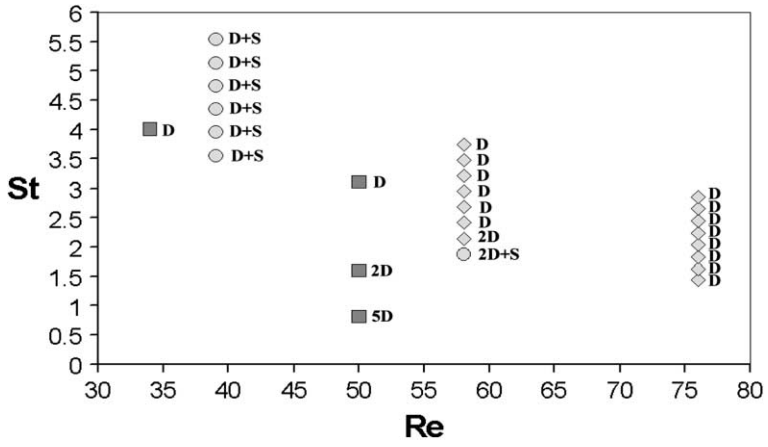

Fig. 10. Pinch-off topology for various *Re–St* combinations. All points were obtained using $\eta_i/\eta_o = 1.6$, except for those marked by "■" where $\eta_i/\eta_o = 0.17$. The symbol D denotes a drop of significant volume, and S denotes the presence of a satellite.

These results are at least partially consistent with the existence of a 'preferred' wavelength for jet instability such as those estimated by Meister and Scheele (1967) using Tomotika's theory for cylindrical jets. Smaller forcing frequencies (and *St* values) clearly support longer wavelengths. If the wavelength becomes significantly longer than the preferred wavelength, however, formation of harmonics resulting in multiple drops or satellites is likely. The relation between satellite formation and Reynolds number is more difficult to explain.

From Meister and Scheele's calculations, the most unstable dimensionless wave number for the parameters we have in our experiment is $(ka)_{max} = 0.664$. The letters k and a correspond to the wave number and jet radius, respectively. In practice, we measured k and a directly from the images acquired during the experiments. The case at $Re = 58$, which corresponds to the forcing frequency of 13 Hz, yielded the dimensionless wave number $(ka) = 0.679$. The case at $Re = 39$, which corresponds to the forcing frequency of 9 Hz, yielded the dimensionless wave number $(ka) = 0.652$. Therefore it is logical that satellites could form at $Re = 39$. In the following paragraphs, the nature of the satellite and drop formation is discussed.

At $Re = 39$, satellites formed for every Strouhal number tested from 3.55 to 5.53. From cycle to cycle, the size of the satellites varied with the largest variation occurring at the lowest Strouhal number (3.55). For this case, the volume ratio between the largest and smallest satellites observed was approximately 7:1. Downstream cone angles (the angle between the downstream cone interface and the horizontal) varied between 4° and 71°. At the same time, jet angles upstream of the cones varied between 53.5° and 72°. Smaller jet and cone angles correspond to the formation of large satellites and vice versa. Note that these jet and cone angles do not represent pinch-off angles as explained in Section 3.1.1. (The actual angles associated with the break between the satellite and primary drop were very difficult to measure.) The largest satellites formed from pear-shaped main drops, medium satellites formed from cone shapes (as in Fig. 3), and the smallest satellites formed from very narrow cones and elongated fluid filaments stretching between the jet and main drop. Similar thin filaments have been observed in liquid/gas and liquid/liquid flows by other researchers (Chaudhary and Maxworthy, 1980; Kowalewski, 1996; Webster and Longmire, 2001).

Increasing the Strouhal number at this Reynolds number decreased the range of satellite drop sizes. Beginning at $St = 4.34$, large satellites occurred very rarely, and the range of cone angles was reduced to 30.5–75°. The corresponding jet angles stayed essentially unchanged, 56–72.5°, compared with the lower St cases. Further increases in St resulted in slightly larger cone angles (44–83°) and no large satellites.

At $Re = 58$, satellites formed only at the lowest Strouhal number examined, $St = 1.87$. At that frequency, a smaller and then a larger drop formed in sequence for every forcing cycle. The larger drop was approximately 4.6 times the volume of the smaller drop. A satellite would subsequently pinch-off from the downstream end of the larger drop resulting in a total of three drops/cycle. At higher Strouhal numbers, no satellites occurred on any regular basis. Measurements of the jet and drop pinch-off angles consequently varied over a relatively small range. Drop pinch-off angles fell between 3.5° and 12°, and jet pinch-off angles fell between 76°and 84°. The same trends occurred at $Re = 76$. At the lowest Strouhal number ($St = 1.43$), the large primary drop that formed would occasionally divide into a larger downstream and a smaller upstream drop. Measurements of drop and jet pinch-off angles fell in the same ranges as for $Re = 58$.

In general, the drop and jet pinch-off angles measured for cases with no satellites agreed within uncertainty with the previous measurements in Longmire et al. (2001) and the boundary integral calculations of dripping flows by Zhang and Lister (1999). This result suggests that, at least for pinch-off of primary drops, the interface pinch-off angles appear to be relatively independent of the Reynolds and Strouhal numbers. For cases that resulted in satellites, the angles associated with the satellite/primary drop break are very difficult to estimate because they may change significantly over very short times before pinch-off. Shortly before the break, the primary drop angle appears negative, but some images suggest that, as pinch-off is approached, the angle may become positive. The upstream interface angle associated with the satellite is also uncertain, but *may* fall in the same range as the jet pinch-off angles listed above.

The points in Fig. 10 corresponding with the lower viscosity ratio ($\eta_i/\eta_o = 0.17$) match the topology trends for $\eta_i/\eta_o = 1.6$ in terms of the number of primary drops formed/cycle. However, no satellites formed (see e.g. $Re = 34$, $St = 4$). For this viscosity ratio, it is likely that the higher ambient viscosity suppresses instabilities on the jet surface and hence the formation of satellites. In fact, no 'harmonic' instabilities or zones of concave curvature have been observed on developing primary drops for this fluid combination.

3.3. Effects of forcing amplitude

Additional laser induced fluorescence experiments were conducted to investigate the influence of perturbation amplitude on satellite formation. In the experiments described in the previous section, the amplitudes were set just high enough to yield a stable pinch-off mode. To determine whether increased forcing amplitudes could suppress satellite formation, we examined all of the cases at $Re = 39$ plotted in Fig. 10. For the four lower Strouhal numbers, satellites persisted even when the system was forced at its upper limit (voltage input to speaker = 19 V). By contrast, the two higher Strouhal numbers ($St = 5.13$ and $St = 5.53$) showed some suppression of satellite formation at large forcing amplitudes.

At $St = 5.13$, a forcing amplitude of 11 V yielded a variation in the mean volumetric flow rate of about 25%. (The variation is measured as one half of the peak-to-peak amplitude.) Satellites

did not form on any regular basis, and any that formed were quite small. Increasing the amplitude to 15 V or higher (corresponding to a volumetric flow variation of 30%) did not change the situation significantly. At the highest Strouhal number ($St = 5.53$), the resulting behavior was similar except for one significant difference. At 19 V (the upper limit of the system performance), satellites disappeared completely. At this forcing level, the variation in volumetric flow rate was 38%. The behavior observed qualitatively matches that seen in liquid/gas flow by Pimbley and Lee (1977). However, it is clear that in the liquid/liquid flow at least, the velocity variations required for satellite suppression are quite large.

In general, the main drop became more rounded as the forcing amplitude was increased. At the highest amplitude, the drop was nearly spherical. The jet column became thicker and shorter since the pinch-off location moved closer to the nozzle. For the case where satellites were completely suppressed, no inverted curvature was observed on the drop interface in contrast to the two cases described in Section 3.1.1. Increases in forcing amplitude also suppressed oscillations of the main drop after it separated from the jet column.

4. Conclusions

In this paper, we examined satellite drop formation and pinch-off transition in liquid–liquid jet systems where gravitational effects, viscosity, inertia, periodic forcing and interfacial tension were all significant. For the fluid combination examined in detail ($\eta_i/\eta_o = 1.6$), satellite formation was associated with lower Reynolds and Strouhal numbers. Visualization and PIV results showed that satellite occurrence depends on the interface shape approaching pinch-off as well as the detailed velocity gradients surrounding the pinch-off region. Satellite formation required the existence of a 'harmonic' (defined by a section of concave curvature) on the interface in the zone that subsequently broke off of the jet tip. In addition, the location of the concave curvature was important. If the concave curvature was located far enough downstream of the jet neck, no satellite developed. By contrast, if the concave section was close enough to the jet neck, the resulting velocity and vorticity pattern deformed the interface into an upstream-facing cone attached to the main drop that subsequently broke off as a satellite.

Increasing the viscosity of the outer or ambient fluid suppressed satellite formation. Also, it was sometimes possible to suppress satellite formation by increasing the forcing amplitude. Both increased ambient viscosity and increased fundamental forcing acted to suppress harmonic waves on the interface surface and hence the conditions required for satellite formation.

Acknowledgements

This work was supported by the Engineering Research Program of the Office of Basic Energy Sciences at the Department of Energy (grant DE-FG02-98ER14869).

References

Bogy, D.B., 1979. Drop formation in a circular liquid jet. Ann. Rev. Fluid Mech. 11, 207–208.

Chaudhary, K.C., 1977. The nonlinear capillary instability of a jet. Ph.D. thesis, University of Southern California, Los Angeles, 220 pp.

Chaudhary, K.C., Maxworthy, T., 1980. The nonlinear capillary instability of a liquid jet. Part 3. Experiments on satellite drop formation and control. J. Fluid Mech. 96, 287–297.

Cohen, I., Brenner, M.P., Eggers, J., Nagel, S.R., 1999. Two fluid drop snap-off problem: experiments and theory. Phys. Rev. Lett. 83, 1147–1150.

Kitamura, Y., Mishima, H., Takahashi, T., 1982. Stability of jets in liquid–liquid systems. Can. J. Chem. Eng. 60, 723–731.

Kowalewski, T.A., 1996. On the separation of droplets from a liquid jet. Fluid Dyn. Res. 17, 121–145.

Lafrance, P., 1975. Nonlinear breakup of a liquid jet. Phys. Fluids 18, 428–432.

Longmire, E.K., Lowengrub, J.S., Gefroh, D.L., 1999. A comparison of experiments and simulations on pinch-off in round jets. In: ASME FEDSM99-7111, 3rd ASME JSME Joint Fluids Engineering Conference, San Francisco.

Longmire, E.K., Norman, T.L., Gefroh, D.L., 2001. Dynamics of pinch-off in liquid/liquid jets with surface tension. Int. J. Multiphase Flow 27, 1735–1752.

Meister, B.J., Scheele, G.F., 1967. Generalized solution of the Tomotika stability analysis for a cylindrical jet. AICHE J. 13, 682–688.

Meister, B.J., Scheele, G.F., 1969. Predictions of jet length in immiscible liquid systems. AICHE J. 15, 689–699.

Nayfeh, A.H., 1970. Nonlinear stability of a liquid jet. Phys. Fluids 13, 841–847.

Pimbley, W.T., Lee, H.C., 1977. Satellite droplet formation in a liquid jet. IBM J. Res. Develop. 21, 385–388.

Richards, J.R., Beris, A.N., Lenhoff, A.M., 1993. Steady laminar flow of liquid-liquid jets at high Reynolds numbers. Phys. Fluids 5, 1703–1717.

Rutland, D.F., Jameson, G.J., 1970. Theoretical prediction of the sizes of drops formed in the breakup of capillary jets. Chem. Eng. Sci. 25, 1689–1698.

Scarlett, B., Parkin, C.S., 1977. Droplet production by controlled jet break-up. Chem. Eng. J. 13, 127–141.

Skelland, A.H.P., Walker, P.G., 1989. The effects of surface active agents on jet breakup in liquid-liquid systems. Can. J. Chem. Eng. 67, 762–770.

Taub, H.H., 1976. Investigation of non-linear waves on liquid jets. Phys. Fluids 19, 1124–1129.

Tjahjadi, M., Stone, H.A., Ottino, J.M., 1992. Satellite and subsatellite formation in capillary breakup. J. Fluid Mech. 243, 297–317.

Webster, D.R., Longmire, E.K., 2001. Jet pinch-off and drop formation in immiscible liquid/liquid systems. Exp. Fluids 30, 47–56.

Yuen, M., 1968. Non-linear capillary instability of a liquid jet. J. Fluid Mech. 33, 151–164.

Zhang, X., Basaran, O., 1995. An experimental study of dynamics of drop formation. Phys. Fluids 7, 1184–1203.

Zhang, W.W., Lister, J.R., 1999. Similarity solutions for capillary pinch-off in fluids of differing viscosity. Phys. Rev. Lett. 83, 1151–1154.